RESIDUAL STRESS CHARACTERIZATION FROM NUMERICAL ANALYSIS OF THE MULTI-PARTICLE IMPACT BEHAVIOR IN COLD SPRAY

Kando Hamiyanze Moonga
Mechanical Engineering Science Department
University of Johannesburg
Johannesburg, Gauteng, South Africa

Tien-Chien Jen
Mechanical Engineering Science Department
University of Johannesburg
Johannesburg, Gauteng, South Africa

ABSTRACT

In cold spray, bonding is created between a substrate and the particles and between particles through impact deformation at high strain rates. A prominent feature of the cold spray process is the compressive residual stress that arises during the deposition process. Compressive residual stress on the surface can be beneficial for fatigue resistance. As a post processing technique several applications require surface treatment processes that produce this state of stress on component surfaces such as shot peening, laser shock peening, ultrasonic impact treatment, low plasticity burnishing, etc. In all of these methods the compressive stress is produced through plastic deformation of the surface region. In a similar manner, the cold spray process induces compressive stress by high speed impact of the sprayed particles on the surface, causing a peening effect. The effects of these variations in the properties of the coatings are rarely reported. Moreover there are some applications which require minimal residual stresses in the components such as in optics. In this study, we have investigated the residual stress using numerical analysis of the multi-particle impact behavior in cold spray.

Keywords: Multiple particle impact, cold spray, Residual stress, surface roughness

INTRODUCTION

The residual stresses in an engineering component can be a factor in the choice of manufacturing method. This can be driven by the need for surface compressive residual stresses or the need for minimal residual stresses in the component. Thin film properties strongly depend on their microstructure parameters such as preferred orientations, grain size, stress and strain values which have important roles in design, production and reliability of different devices [11]. For example inherent stresses in optical components influence the polarization of light by stress birefringence, an effect that is undesirable in demanding applications such as microlithography, laser optics and astronomy [1]. Mechanical stresses induced in the optical material due to manufacturing processes lead to deformations in the material structure and thus to different particle densities along axes.

NOMENCLATURE

A, B, C	material specific constants
K	stress optical coefficient [mm^2/N]
T	temperature [C]
d	light path in the sample [mm]
m, n	material specific constants
p	pressure stress [N/mm^2]
q	Mises stress[N/mm^2]
$d_1, d_2, d_3, d_4\ d_5$	material failure related parameters
σ	stress (residual stress) [N/mm^2]
σ_d	deposition stress
$\Delta\varepsilon_t$	change in thermal stress
ΔT	change in temperature
$\Delta\alpha$	thermal expansion coefficient difference between two materials
G_f	fracture energy per unit area [J/m^2]
$\bar{\sigma}$	material yield flow stress

Abbreviations

OPD	optical path difference [mm]
SBR	stress birefringence

Greek symbols

$\bar{\varepsilon}_p$	effective plastic strain
$\dot{\bar{\varepsilon}}^{pl}$	plastic strain rate [/s]
$\dot{\varepsilon}_0$	reference strain rate [/s]
ω	material damage parameter

The difference in the optical path (OPD) inside a material sample can be represented as

$$OPD = K.d.\sigma \quad (1)$$

Where K is the stress optical coefficient (mm^2/N) or photoelastic constant (10-12 Pa, or Brewster) of the material, d is light path in the sample, and σ is the mechanical stress. For instance the image of Fig. 1 shows the stress birefringence distributions in the optical glass CaF2 disk [2]. Residual stress (or stress birefringence, SBR) is a major design parameter in optics. Tolerable residual stresses in such components can be chosen to be in a specific range based on excitation waves. In addition high stress levels in thin film coatings have been found

to cause delaminating of the coatings. Whilst residual stress can be undesirable in optics, it is a desirable feature in mitigation of fatigue life of engineering components. Hence shot peening process is used to add compressive residual stresses to engineering components exposed to high fatigue loading.

Various state of the art residual stress measurement methods exist in industry. Most of these are listed by the Society for Experimental Mechanics such as neutron diffraction, ultrasonic, magnetic methods, x-ray diffraction, etc. The ASTM has some standard test methods such as hole-drilling and x-ray diffraction methods. The choice for a measurement method can be driven by the need to meet specific characteristics of the process and of the substrate material involved, for example stress in glass cannot easily be measured by the standard x-ray diffraction method because of its amorphous structure. The other determining factor in the choice of residual stress measurement method would be the need for a non destructive analysis.

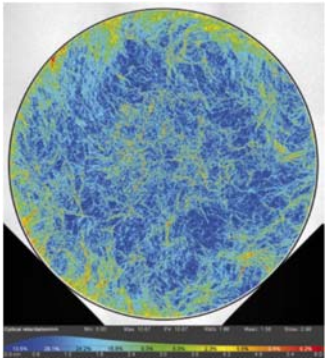

Figure 1. Distribution of the SBR intensities: Result stitched together from nine single measurements of a CaF2 disk 240 mm in diameter [2]

In cold spray experiments, the residual stress profiles have previously been interpreted by fitting them using Tsui and Clyne's progressive coating deposition model [3, 7]. This model was originally developed for thermal spray accumulative residual stress modeling in the coatings. It is reported that the model works equally well for cold spray coatings [7]. This model comprises two components of the spray process that are accounted for separately using two different fitting parameters: The first fitting parameter arises from the coating deposition process being considered as the formation of a new layer on the top of the system comprising all of the previously sprayed layers, plus the substrate [7]. This new layer is formed with a characteristic deposition stress σ_d. For cold spray coatings this stress is compressive, characteristic of a peening process whereas in thermal spray its mainly tensile. The second parameter, $\Delta\varepsilon_{th}$ accounts for any thermal expansion coefficient mismatch between the substrate and coating materials, given as $\Delta\varepsilon_{th} = \Delta\alpha\Delta T$. The significance of this term depends on the cooling range and difference in thermal expansion coefficients between the coating and substrate materials.

Analysis of the experimentally measured stress profiles in terms of the model allows separation of σ_d and $\Delta\varepsilon_{th}$, and their relative significance can be determined for a given coating-substrate system quantitatively. This separation can be used to assess the importance of the thermal vs. kinetic (peening) components of the coating process, and the sensitivity of a given system to the accumulation of residual stress. The characterization of a particular spraying process by σ_d and $\Delta\varepsilon_{th}$ parameters, allow for prediction of stresses in other systems, such as the use of different thickness or different materials.

RESIDUAL STRESS ANALYSIS

The current desire to have cold spray of functional thin films requires the understanding of the coating process in much finer level. This has the advantage that specific properties can be understood a priori in the coatings whilst methods to reduce undesired properties can be developed. Yildirim et al. [4] studied residual stress distribution in a single particle impact using numerical modeling at velocities 100, 300, 500 and 700m/s. They found that the magnitude of the residual stress were close to work hardening strength of OFHC (Oxygen-free high thermal conductivity) copper which is around 400MPa and is calculated from the Johnsons-Cook equation. For the velocity range of between 500 to 700m/s the levels of tensile stresses were observed around the surface following the jetting area.

In experimental investigations of residual stress analysis, XRD methods are reported in cold spray coating analysis of the surface layer using an AST X-Stress 3000 diffractometer [7,13]. With this instrument, the effective penetration depth of the radiation is said to be approximately 5µm. Using this equipment residual stress measurements can be performed in the coating depth in the subsurface by step increment at each step starting with electro-polishing a thin layer to expose the inside depths of the coatings followed by the stress measurement. The measurements are reported to have been done in three different orientations of 0, 45 and 90 degrees [7]. The particles for deposition can be analyzed with laser diffraction, for the size distribution. X-ray diffraction methods have also been used to evaluate residual stress in thin film coatings on optical substrates. For instance a high temperature XRD instrument was used in residual stress analysis of a silver thin film coating with 80nm thickness [12].

On the numerical modeling of residual stress, it was observed that the main challenges to develop a numerical model representing the cold spray process is the correct estimation of the distribution of the particle size and impact position [7]. For the numerical model the bottom side face of substrate can be meshed by half infinite elements to provide quiet boundaries by minimizing the reflection of dilatational and shear waves back in to the region of interest [7, 11].

Evaluating the coating residual stress and the coating relaxation behavior after thermal treatments is imperative to establish the reliable functionality of the coating for the proposed application [10]. A detailed understanding of parameters involved for specific type of coating will enable specialized coating processes for specific applications. In addition, specialized equipment using cold spray method would be designed and can further be automated for specialized functions.

This study focused on the residual stress distribution and the surface roughness properties of the generated coatings in cold spray using numerical modeling. The investigation involved a numerical modeling analysis and further examined experimental data and literature related to the subject.

NUMERICAL SIMULATIONS

Numerical simulations are a vital tool in modern advanced research and systems design as they are used to predict properties some of which can be difficult to examine experimentally. In addition numerical methods are a quick guide in decision making especially in new equipment design, process optimization or theoretical validation. Specifically, in this study numerical methods were applied to investigate various modalities of the cold gas spray coating process so as to find what parameters can be improved on the coating experimental models. ABAQUS CAE/FEM was used in the numerical simulations to predict the residual stress distribution. The next section discusses the material constitutive models that were used in the ABAQUS numerical investigations done in the study of film coating process to examine the residual stress distribution and size variation in the physical structure.

CONSTITUTIVE MODELS AND MATERIAL BEHAVIOR

In metal plasticity Johnson-Cook models have been extensively used to define the material behavior. The material model for both the particles and the substrate were described using the Johnson-Cook plasticity model. In the Johnson-Cook model the yield flow stress, $\bar{\sigma}$ of the material is expressed as follows

$$\bar{\sigma} = [A + B(\bar{\varepsilon}^{pl})^n]\left[1 + C\, ln\left(\frac{\dot{\bar{\varepsilon}}^{pl}}{\dot{\varepsilon}_0}\right)\right]\left(1 - \hat{\theta}^m\right) \qquad (2)$$

where A, B, n, C, and m are material specific constants, $\bar{\varepsilon}_p$ is the effective plastic strain, $\dot{\bar{\varepsilon}}^{pl}$ is the strain rate, $\dot{\varepsilon}_0$ is the reference strain rate, $\hat{\theta}$ is the dimensionless temperature defined as:

$$\hat{\theta} \equiv \begin{cases} 0 & for\ T < T_{transition} \\ \dfrac{(T - T_{transition})}{(T_{melt} - T_{transition})} & for\ T_{transition} \le T \le T_{melt} \\ 1 & for\ T > T_{melt} \end{cases} \qquad (3)$$

where T is the current temperature, T_{melt} is the melting temperature of the material, and $T_{transition}$ is the transition temperature below which there is no temperature dependence on the resultant yield stress. The actual parameters used in the numerical simulation for the two materials are given in Table I.

Table I Properties of copper [8], Aluminum [9]

Material	Cu	Al
Density, Kg/m^3	8960	2710
Thermal Conductivity, W/(m□)	386	220
Specific Heat Capacity,]/Kg□	383	920
Melting Point, □	1083	643
Elastic Modulus, GPa	124	65.762
Poisson's ratio	0.34	0.3
JC Plasticity: *A*, MPa, *B*, MPa, *n*, *C*, *m*	90, 292, 0.31, 0.025, 1.09	148.361, 345.513, 0.183, 0.001, 0.859
JC Damage: d1, d2, d3, d4, d5	0.54, 4.89, -3.03, 0.014, 1.12	0.071, 1.248, -1.142, 0.147, 1
Reference Temperature, □	25	25
Reference Strain, 1/*s*	1	1

The coupling in the solving of the heat transfer equations was set such that 90% viscoplastic work is converted into heat by setting inelastic heat constant in ABAQUS to 0.9. Frictional contact was modeled as coulomb friction with 0.2 frictional coefficients in Model 1 and Rough contact formulation in Model 2.

Johnson-Cook (JC) Dynamic Failure Model

Material failure in the Johnson-Cook model can be modeled as either a power law or exponential law. The onset of material failure can be specified. The modeling behavior involves damage initiation and damage evolution. ABAQUS/Explicit has the general implementation of the Johnson-Cook failure model as part of the family of damage initiation criteria, which can be used in modeling progressive damage and material failure and is the recommended technique in high dynamic impact analysis. The Johnson-Cook dynamic failure model is based on the value of the equivalent plastic strain at element integration points; failure is assumed when the damage parameter exceeds 1. The damage parameter, ω, is defined as:

$$\omega = \sum\left(\frac{\Delta\bar{\varepsilon}^{pl}}{\bar{\varepsilon}_f^{pl}}\right) \qquad (4)$$

where $\Delta\bar{\varepsilon}^{pl}$ is an increment of the equivalent plastic strain, $\bar{\varepsilon}_f^{\mathrm{pl}}$ is the strain at failure. The summation is performed over all increments in the analysis. The strain at failure, $\bar{\varepsilon}_f^{\mathrm{pl}}$, is assumed to be dependent on a nondimensional plastic strain rate, $\dot{\varepsilon}^{\mathrm{pl}}/\dot{\varepsilon}_0$; a dimensionless pressure-deviatoric stress ratio, p/q (where p is the pressure stress and q is the Mises stress); and the dimensionless temperature, $\hat{\theta}$, defined earlier in the Johnson-Cook hardening model. The dependencies are assumed to be separable and of the form

$$\bar{\varepsilon}_f^{pl} = \left[d_1 + d_2\, exp\left(d_3\frac{p}{q}\right)\right]\left[1 + d_4\, ln\left(\frac{\dot{\bar{\varepsilon}}^{pl}}{\dot{\varepsilon}_0}\right)\right]\left(1 + d_5\hat{\theta}\right) \qquad (5)$$

where $\mathrm{d}_1 \sim \mathrm{d}_5$ are failure parameters measured at or below the transition temperature, $\theta_{\mathrm{transition}}$, and $\dot{\varepsilon}_0$ is the reference strain rate. These parameters are given in table I for the simulation in this study.

When the failure criterion is met, the deviatoric stress components are set to zero and remain at zero for the rest of the analysis. Depending on the choice, the pressure stress may also be set to zero for the rest of calculation (if this is the case, the element will be deleted) or it may be required to remain compressive for the rest of the calculation (if this is the case, the element should not be deleted). By default, the elements that meet the failure criterion are deleted. The fracture energy per unit area can be specified by, $\mathrm{G_f}$, to be dissipated during the damage process directly. Instantaneous failure will occur if $\mathrm{G_f}$ is specified as 0; however, this choice is not recommended and should be used carefully because it causes a sudden drop in the stress at the material point, which can lead to dynamic instabilities.

COMPUTATIONAL MODEL (FEA)

In computational mechanics, a problem is set by building the physical model, specifying the boundary conditions and the

initial conditions. In the next section we look at the computational models.

Multi - Particle Simulation

Two problem sets were studied using ABAQUS CAE finite elements modeling. This was to study the behavior of the multiple particle impact which is prevalent in generation of coatings using cold gas dynamic spray technology. Initial particle velocities and initial temperatures were specified for each problem investigation. In the first case study a 2D element model was used and surface interaction was defined between any two interacting particles and the substrate to each particle. An encastre support on bottom of substrate was imposed, the sides were also supported. The infinity boundary condition was not possible with the elements used in the 2D mesh.

In the second Model, (model 2), 3D thin elements constrained in the z-direction to create a 2D model are used to take advantage of the use of the general contact model in defining the particle to particle interaction and the infinity boundary condition. In this model infinity boundary conditions are used. The material set, the initial temperatures and initial velocity were kept as before.

Model 1: In this setup, the instant locations with reference to the substrate are given as Fig 2.

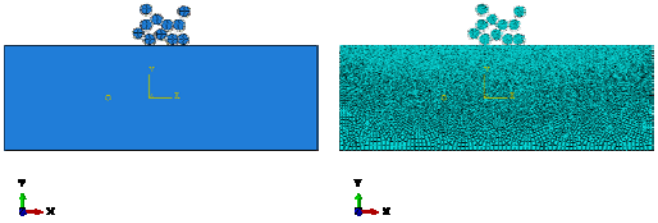

(a) (b)

Figure 2. Computational domain, Model 1 (a) initial and boundary conditions; (b) meshing domain (resolution of 1/40dp, dp= 10µm particle diameter in the micro units).

ABAQUS solves the dynamic temperature displacement problem which accounts for various energy forms in the computation. In Model 1, CASE1 Adhesion forces and cohesion forces resulting from the interaction of particles and the substrate were not modeled. In CASE2 adhesion force is modeled by assuming a 100% deposition while CASE1 no adhesion forces are used and modeling result is obtained at subsequent restitution. In view of that the simulation results are only observed in the time of impact and duration of deformation. This is up to the onset of subsequent restitution.

In Model 2, 3D elements were used and constrained in the z-direction to simulate a 2D problem. Infinity boundary condition is used. Adhesion is modeled by assuming a 100% deposition. In all models the impact velocity used is 500m/s, the initial temperature of the particles and substrate was 25 degrees Celsius. **Model 2** setup of the instance locations with reference to the substrate are given as Figure 3.

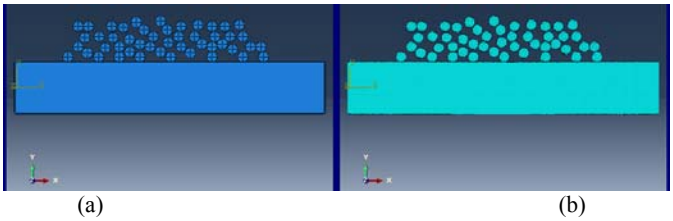

(a) (b)

Figure 3. Computational domain, Model 2 (a) initial and boundary conditions; (b) meshing domain (resolutions of 1/20dp and 1/50dp; dp= 10µm particle in the micro units).

SIMULATION RESULTS

Pressure stress distribution and normal stress in global y-axis

In ABAQUS, residual stresses in the 2D numerical model have been previously analyzed and visualized either using pressure stress or normal stresses for the depth stress. In terms of the pressure stress, the positive values indicate compressive stress while the negative values indicate the tensile stresses. Fig. 6 (a) is the result of the pressure stress obtained in the multi-particle model 1. According to ABAQUS manual, Element deletion can have effects in the pressure stress values upon material failure depending on the settings [12]. This was not used and the two residual stress distributions using the pressure stress results and the normal stress are shown on Fig. 6 (a) and Fig. 6 (b), respectively.

For the normal residual stress in y-direction, the negative values are compressive while the positive values are tensile. The jetting areas are seen to have tensile residual stresses; in addition the interfaces inclined away from the horizontal are showing tensile residual stresses. The interfaces that are closely aligned to the horizontal axis are more compressive. The particle internals have both compressive and tensile stress regions inclined at some angle away from the vertical. These results were obtained without modeling adhesive force in the numerical model.

(Stress values: $x10^{-3}MPa$)

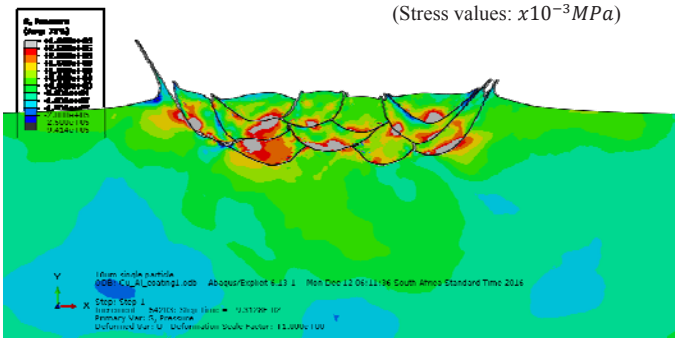

(Stress values: $x10^{-3}MPa$)

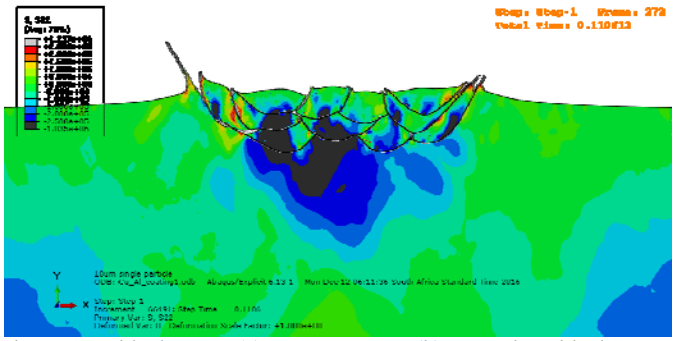

Figure 6 Residual Stress, (a) Pressure stress; (b) Normal Residual Stress (y-direction in global axis)

Stress line Analysis (stress linearization in the depth of the coating-substrate system)

Residual Stress distribution for the coating and substrate is analyzed in this section in terms of normal stresses. When you apply the Stress Linearization, Abaqus/CAE creates an X–Y plot of the chosen stress component; in this case the S22 stress component is oriented normal to the stress line [12]. Therefore the residual stresses in this section are given in two different coordinate systems, one being a local coordinate system and the other distribution in global coordinate system.

In terms of local coordinate, a stress line defined from the model as shown in Fig. 7 starts from the surface into the depth of the substrate of the simulated coating and the resulting profiles are as shown for Model 1 and Model 2 respectively.

Model 1 CASE 2 Analysis

A compressive zone observed through the depth of the coating and substrate. This could be attributed to the type of boundary support and size of the substrate. In this study, the thickness of the simulated substrate was only 100 µm in depth, Model 1, with supported boundary condition at the base this depth is not much to give a complete residual stress mapping to the zero induced residual stress regions into the depth of the substrate. The line membrane stress in x-direction indicates a value of about -165MPa, for the entire systems, that is for the substrate and for the coating as observed in Fig. 7 (a). For the stresses in the y-direction, a line membrane stress of -275MPa is observed in Fig. 7 (b). In this model a large compressive region is observed into the substrate. This could be due to the encaster supports.

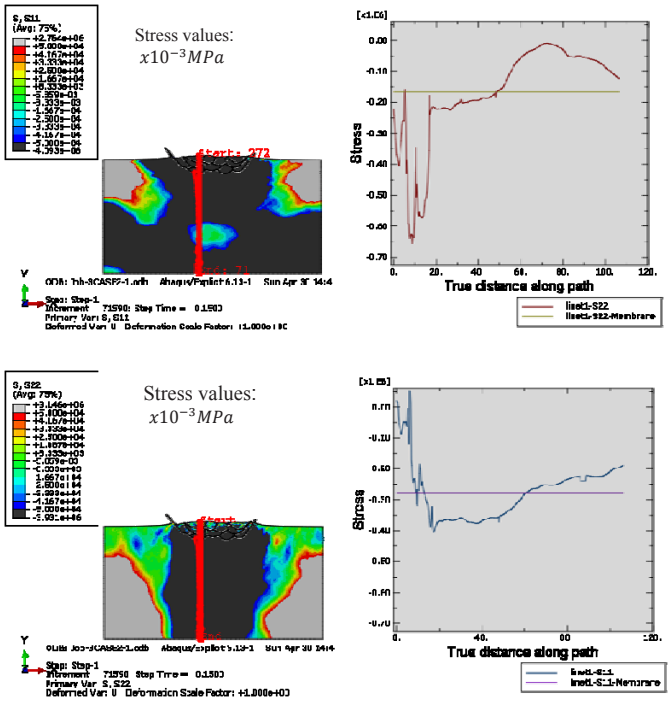

Figure7. Residual Stress: in-depth stress variation (in the local axis normal to indicated line), and pressure stress variation on the global coordinate axis shown

Model 2 Analysis

Figure 8 is a comparison of the fine and coarse mesh in the computational model. At 133ns time step after impact, the residual stress did not give a significant difference for a general trend, and moreover the quantitative values were observed to be same as seen in the stress curves shown.

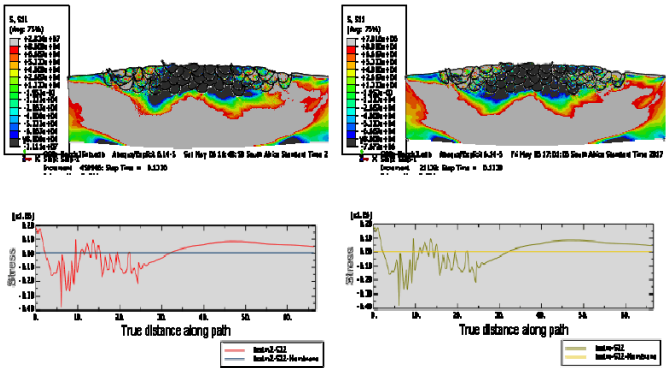

(a) (b)

Figure 8. Residual stress distribution (a) Model 2 with mesh resolution of 1/50dp, Showing up to 133ns after impact (b) Model 2 with Mesh resolution of 1/20dp at 133ns after impact.

In the two results for fine and course mesh, the residual stress curves in the coating still show no significant difference at 133ns after impact. As the fine mesh model was incomplete, the course mesh (1/20dp) was used in the subsequent analysis.

Meanwhile the results in Fig. 9 and 10 are obtained at 300ns after impact in the course meshed analysis. This study also shows how the stress waves move during the transient state of the impact process, giving an overall picture of the impact process.

Figure 9 shows for Model 2 residual stress distributions in the numerical simulation based on global coordinates (Fig. 9 (a)) and the linearized stress in the given local axis (Fig. 9 (b)). The residual stress in the local axis shows a mixture of tensile and compressive stresses within the particles. Residual stress in the x-direction in the substrate shows a compressive region followed by a tensile stress far in the depth of the substrate. As observed in the line membrane stress, the linearized residual stress indicate a value of about zero for the entire system of substrate and particles, while for the substrate only a tensile stress (45MPa) and for the coating a compressive stress (45MPa).

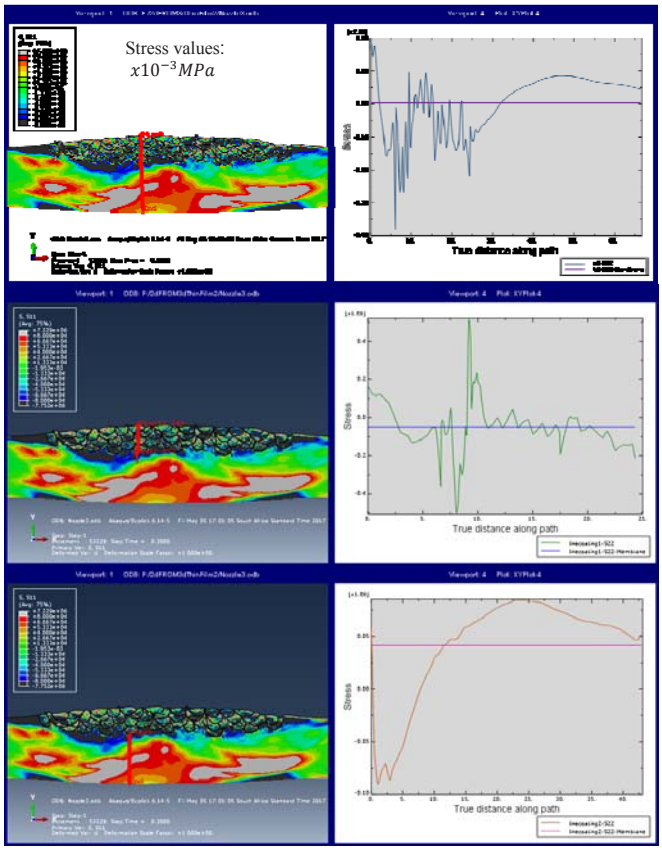

(a) (b)

Figure 9. Residual Stress: (a) stress variation x-axis direction on the global coordinate axis shown (b) in-depth stress variation (in the local axis normal to the indicated line in (a)) (Model 2 mesh size 1/20dp)

In Fig. 10, the linearized stresses in the particles have high compressive and tensile stresses in the range of -310MP to +450MPa with zero membrane stress. In the substrate this range is from -5MPa to +110MPa and 15Pa membrane stress. On a global scale the stress variations can be observed in the images shown. The values given here are for only a single stress line on the integration point in the numerical analysis and were not averaged.

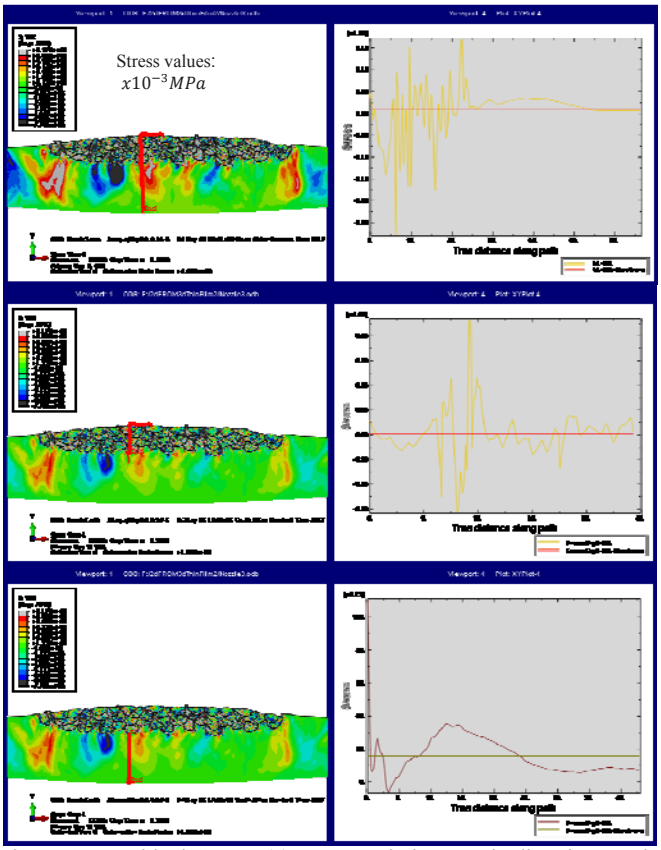

Figure 10. Residual Stress: (a) stress variation y-axis direction on the global coordinate axis shown (b) in-depth stress variation (in the local axis along the indicated line in (a)) (Model 2, mesh size 1/20dp)

Residual stress analysis in the substrate, the coating and the interface and surface

Residual stress distribution (in the global coordinate systems shown), The Fig. 11 is based on Model 1, CASE1 (without modeling the adhesive forces). Similar to the result of a single particle in [4], the multi-particle model for a single-pass shows some symmetrical stress distribution in a single pass coating. In a macroscopic view a compressive region is seen curving into the substrate from one peripheral and protruding towards the other end. The substrate interface residual stress is observed to be as shown in Fig. 11. It varies from tensile at the peripheral due to jetting, and then most of it remains highly compressive with minor tensile stresses observed depending on the roughness profile either sagging or hogging. On the crater of the sagging profile the stresses are tensile, while on the peak of the hogging profile, the stresses are observed to be compressive. Such an anlysis can be useful in understanding how high stresses are generated and how these can be mitigated for the cold spray coating process.

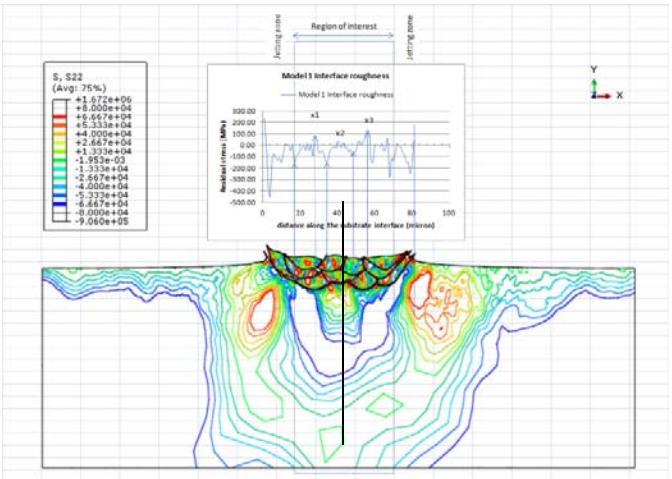

Figure 11. Residual stress at the substrate interface profile in the y-direction (Model 1 CASE1, hour glassing used which reduced substantial jetting in the substrate)

As the numerical analysis is based on a 2D model, the substrate tensile residual stress observed at the surface in the region of interest could be located in a very centralized surface area in the 3 dimensional analysis. It is also observed that this residual stress occurs more like a spike along the surface. Most part of the substrate interface residual stress is therefore compressive and the average value was found to be -59.5MPa for the entire length; not only the region of interest but also the jetting region as shown in the Fig. 11.

The Figures 6 - 11 also give a global view of the coating process and how the stress waves are aligned in the cross section of the single pass coating; compare this with a single particle model. This gives a macroscopic view of the residual stress distribution in the substrate component and the coating. The residual stresses can be observed in the various scales including particle interfaces, jetting, and internal alignment in the particles; it also shows the preferred distributions of the compressive and tensile residual stresses in the particles.

Comparison with similar studies and some experimental investigations

When comparing experimental data and numerical simulations it becomes important to consider the various assumptions and limitations in the numerical modeling analysis used. In this numerical study, a 100% deposition efficiency is used. There could be a possibility that the deposition efficiency has effect on the final residual stresses. In that case deposition efficiency could act as a level of shot peening process on the already deposited particles. Fig. 12 shows the surface effects of a deposition efficiency far much less than 100%, an image with bonded and non-bonded particles. Impact locations where bonding did not occur show craters whereas the positions where particle bonding occurred show the embedded particles. Craters create some sort of shot peening which can occur on the already deposited layers of particles.

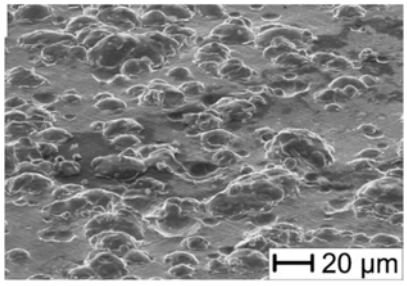

Figure 12. Scanning electron micrographs (secondary electron mode) of wipe test samples of copper particles on a copper substrate, showing an overview (extract from Assadi et al. [5])

In literature the residual stress state of the coatings was found to depend mainly on the deformation behavior and properties of the coating material and the kinetic parameters of the cold spray process [6]. Another contributing factor in residual analysis is that of the thickness of the coating or the number of passes which creates high density with coating depth. This effect is also explained by the Tsui and Clyne's progressive coating deposition model as discussed earlier. Another parameter is the thermal expansion which was not included in the material behavior.

Quantitative data on the experimental residual stresses for copper impact on aluminum are reported to be -85 ± 20 MPa [6] and -77.3 to -107.5 MPa [4]. In the numerical analysis, for the coating a membrane compressive stress of -45MPa in model 2 is obtained, whilst -165MPa in Model 1 CASE 2 is obtained. Furthermore, the experimental study in [6] found that the residual stress is much larger in the Cu coatings, namely, σ_d, than in Al. This trend is also observed in the current numerical study. In the numerical analysis, the magnitudes of the tensile and compressive stress levels are observed to be much higher to about 400 to 450MPa. These values are similar to the numerical study by Yildirim et.al. [4] in which study it was observed that this is close to work hardening of the copper material. We further not that the high stresses are mainly observed at the particle interfaces.

Meanwhile, this study looked at the possible difference between the numerical model and the experimental coating process. Therefore the study sought to understand detailed numerical modeling of residual stress and the parameters that possibly have effect on the final residual stress levels arousing questions for further investigations. In addition, orientation of residual stress iso-surface contours can be observed and the stress levels in these regions can be predicted and whether compressive or tensile. Stress orientation has coupling effects in optics, where light interacts with material. The results of this study can be used to predict the functions of the film as well as optimize the experimental models used in the cold gas coating process.

CONCLUSION

Residual stress analysis in the numerical modeling of cold spray has the potential to give a better understanding of the relationship between deposition behavior and residual stress

distribution and orientation. Furthermore, the level of deposition efficiency (unsteady flux density) during the coating process creates a certain level of embedded (or hidden) shot peening process whose effects on the coating is not yet investigated. A study of the influence of such coating behavior (embedded shot peening process) will give some more details on the residual stresses at different deposition efficiency. The understanding of these coating process parameters and their influence on residual stress gives the possibility of specialized coating conditions for given surface requirements.

The numerical model in this study gives a guide on the magnitudes of the residual stresses and possibly how they are generated and aligned in the coating thickness. This should match the behavior as observed in experiments. Furthermore, the residual stresses have been analyzed with respect to the roughness morphology; this has been missing in the literature in the numerical modeling analysis.

REFERENCES

1. Katte, H., 2009. Imaging measurement of stress birefringence in optical materials and components. *Photonik international*, *1*(2009), pp.39-41.
2. Katte, H., 2009. Measuring of High Quality Optics for Lithography. *Optik & Photonik*, *4*(2), pp.26-29.
3. Suhonen, T., Varis, T., Dosta, S., Torrell, M. and Guilemany, J.M., 2013. Residual stress development in cold sprayed Al, Cu and Ti coatings. *Acta Materialia*, *61*(17), pp.6329-6337.
4. Yildirim, B., Muftu, S. and Gouldstone, A., 2011. Modeling of high velocity impact of spherical particles. *Wear*, *270*(9), pp.703-713.
5. Assadi, H., Gärtner, F., Stoltenhoff, T. and Kreye, H., 2003. Bonding mechanism in cold gas spraying. *Acta Materialia*, *51*(15), pp.4379-4394.
6. Luzin, V., Spencer, K. and Zhang, M.X., 2011. Residual stress and thermo-mechanical properties of cold spray metal coatings. *Acta Materialia*, *59*(3), pp.1259-1270.
7. Ghelichi, R., Bagherifard, S., MacDonald, D., Fernandez-Pariente, I., Jodoin, B. and Guagliano, M., 2014. Experimental and numerical study of residual stress evolution in cold spray coating. *Applied Surface Science*, *288*, pp.26-33.
8. Gupta, N.K., Iqbal, M.A. and Sekhon, G.S., 2006. Experimental and numerical studies on the behavior of thin aluminum plates subjected to impact by blunt-and hemispherical-nosed projectiles. *International Journal of Impact Engineering*, *32*(12), pp.1921-1944.
9. Guosheng, H., Daming, G., Xiangbo, L. and Lukuo, X., 2014. Effect of the Compressed Layer on Final Impacting Velocity of Submicron Size Particles in Cold Spraying by Computational Methods. *Journal of Computational and Theoretical Nanoscience*, *11*(3), pp.840-846.
10. Srinivasan, D., 2016, High Pressure Cold Spray: Advanced Characterization, *ASM International,* pp.121 - 172 (52)
11. Zolanvari, A., Hasansagha, S., Eshaghi, F., Shahedi, Z. and Zendehnam, A., 2016. Microstructure and Residual Stress Measurement of Ag/Glass Thin Films Using In-Situ High-Temperature X-ray Diffraction. *Armenian Journal of Physics*, *9*(1), pp.15-19.
12. ABAQUS, U., 2014. Version 6.14-1. *Dassault Systémes Simulia Corp., Providence, RI*.
13. Moridi, A., Gangaraj, S.H., Vezzù, S. and Guagliano, M., 2014. Number of passes and thickness effect on mechanical characteristics of cold spray coating. *Procedia Engineering*, *74*, pp.449-459.